How much attenuation at W and Ka bands is caused by melting layer? An answer from multi-frequency radar Doppler spectra

Haoran Li[1] and Dmitri Moisseev[1,2]

[1]*University of Helsinki, P.O. Box 3, Helsinki, Finland*
[2]*Finnish Meteorological Institute, P.O. Box 503, Helsinki, Finland*
(Dated: 22 June 2018)

1 Introduction

Melting layer is known as an area with enhanced radar reflectivity factor in centimeter radar measurements. This enhancement, so-called bright band, is mainly due to the fast increase of the dielectric constant of the melting snow. The bright band feature is significant for radars operating at S, C and X bands, but less obvious for Ka- and W-band radars, at which the dip of reflectivity in the melting layer is reported and known as dark band (Kollias and Albrecht, 2005; Sassen et al., 2005). Accompanied with the weakening bright band when the radar wavelength moves towards millimeter, signal attenuation in the melting layer becomes a knotty problem. The unknown melting layer attenuation blocks the retrieval of ice cloud above for ground-based cloud radars (Illingworth et al., 2007), and hinders the interpretation of rainfall for space-borne radars operating at Ka and W bands which provide global observations from the top to down (Stephens et al., 2002; Hou et al., 2014; Illingworth et al., 2015).

It is believed that if the melting layer model could reproduce the radar reflectivity correctly, the melting process described in the model is confidential. A lot of works have been devoted into develop realistical models to predict microphysical processes inside the melting layer (e.g., Fabry and Zawadzki, 1995; Szyrmer and Zawadzki, 1999; Leinonen and von Lerber, 2018). Matrosov (2008) derived melting layer attenuation relation for X, Ka and W bands based on the existing melting layer models, and matched the model output with X band radar reflectivity profiles. However, Fabry and Szyrmer (1999) found that the bright band model is very sensitive to the assumed electromagnetic properties. Johnson et al. (2016) demonstrated that the electromagnetic properties of the melting snow are highly uncertain because of the water distribution inside. Thus, actual measurements are imperative for better understanding the physical processes in the melting layer as well as constraining the models.

Bellon et al. (1997) determined the melting layer attenuation at X band by the combination of X band and UHF radar measurements. von Lerber et al. (2015) estimated the melting layer attenuation at C band when the melting layer reaches the ground. Recently Nakamura et al. (2018) derived the melting layer attenuation at Ka band via a dual Ka-band radars deployment. However, there is no measurement study on W band melting layer attenuation.

Due to the large data volume, the potential of radar Doppler spectra was not fully investigated in the past. In addition, the combination of radar measurements at different frequencies was demonstrated to reveal more underlying microphysical information (Sekelsky et al., 1999). Tridon et al. (2013) retrieved the rain attenuation at W band by utilizing the flat Rayleigh regime in Ka-W dual-wavelength Doppler spectra ratio. The Rayleigh scattering regime in multi-frequency radar Doppler spectra is also reported in snow by Kneifel et al. (2016). Can we use the Rayleigh regime in multi-frequency radar Doppler spectra to determine the melting layer attenuation at Ka and W bands? This paper provides a roadmap to answer this question.

2 Data

From February to September 2014 Biogenic Aerosols Effects on Clouds and Climate (BAECC) field campaign was carried out at the University of Helsinki Hyytiälä Station (Petäjä et al. 2016),. Dual-frequency (X/Ka) and dual-polarized scanning Atmospheric Radiation Measurement (ARM) cloud radar (X/Ka-SACR) and the zenith-pointing W band ARM cloud radar (MWACR) were deployed during BAECC. The range gate spacing for X/Ka-SACR is 25 m, and 30 m for MWACR. The X/Ka-SACR radars were running different scanning modes during BAECC, we use the vertical pointing data during the precipitation event 12th June 2014 in this study. The original temporal resolution (2 s) is averaged into 1 min for all radar data. More details about the radar products are referred to (Kneifel et al., 2015) and (Petäjä et al. 2016). Radar reflectivity is calibrated by matching the lowest reflectivity to the reflectivity simulated from the video distrometer. Gaseous attenuation is corrected by using the sonding data as input to the millimeterwave propagation model (Liebe, 1985). Since the mispointing of MWACR leads to horizontal shift of W band spectrum, we adopt the method proposed by Kneifel et al. (2016) to correct the W band spectrum by matching the Rayleigh regime of W band to that of Ka band.

3 Method

3.1 Theoretical basis

Regarding the attenuation effects, the measured radar reflectivity factor for a radar operating at the wavelength of λ at the range of *r* can be expressed in the following form (Tridon et al. 2013),

$$Z_{m,\lambda}(r) = Z_{e,\lambda}(r) - 2\int_0^r \alpha_\lambda(s)ds \quad (3.1)$$

where $Z_{e,\lambda}$ is the equivalent radar reflectivity factor, α_λ is the one-way specific attenuation including the attenuation from gases, hydrometeors, and wet radome at the wavelength of λ. Dual-wavelength ratio (DWR) between radars operating at two wavelength λ_1 and λ_2 ($\lambda_1 > \lambda_2$) is defined as,

$$DWR(r) = Z_{m,\lambda_1}(r) - Z_{m,\lambda_2}(r) \quad (3.2)$$

Thus,

$$DWR(r) = Z_{e,\lambda_1}(r) - Z_{e,\lambda_2}(r) + 2\int_0^r [\alpha_{\lambda_2}(s) - \alpha_{\lambda_1}(s)]ds \quad (3.3)$$

where the first and the second terms correspond to Mie scattering effect, and the third term is the attenuation effect. For centimeter-wavelength where most raindrops and snowflakes are good Rayleigh scatters, the Mie scattering effect is 0. After matching the reflectivities from two radars at the bottom of the melting layer, the melting layer attenuation at the higher frequency can be derived after separating the gaseous attenuation. The DWR technique was used to quantify X band melting layer attenuation (Bellon et al., 1997) since most hydrometeors are Rayleigh scatters at X band. However, when it comes to millimeter wavelength, the DWR technique may not be applicable due to the Mie scattering.

3.2 Rain attenuaiton

Nevertheless, there are still small hydrometeors which fall in Rayleigh scattering regime in the millimeter-wavelength radar projected volume. Tridon et al. (2013) demonstrated that the Rayleigh regime in dual-wavelength Doppler spectral ratio (DSR) can be used to untangle the rain attenuation and Mie effect at W band. As shown in Figure 1, the spectrums for X- and Ka-band radars are very similar though the Mie scattering effect starts to emerge when the velocity exceeds 8 m/s. The Mie effect on W band is significant as indicated by the significant dip at around 6.8 m/s in W band spectra. The flat plateau in Ka/W DSR is characterized by the falling velocity within 4 m/s as reported in (Tridon et al., 2013). The flat part in X/Ka DSR is also obvious though a bit noisier. It should be noted that the combination of X and W bands is not applied this study, since the sensitivity of X-band radar is not as good as Ka-band radar and might obscure the Rayleigh regime. The Ka/W DSR in Rayleigh regime at the range of *r* is defined as,

$$DSR_{Rayleigh}(Ka,W,r) = \frac{\int_{v_{Rayleigh,rain}}^{v_{noise,W}} [S_{Ka}(v) - S_W(v)]dv}{v_{noise,W} - v_{Rayleigh,rain}} \quad (3.4)$$

where S_{Ka} and S_W indicate power spectral density at Ka and W bands respectively, $v_{noise,W}$ and $v_{Rayleigh,rain}$ represent the minimum and maximum velocity range in the Rayleigh regime respectively. To ensure the data quality, $v_{noise,W}$ is determined where the power spectral density is 10 dB above the W-band noise level. $v_{Rayleigh,rain}$ is set to 4 m/s. Similarly, the X/Ka DSR in Rayleigh regime for rain at the range of *r* is defined as,

$$DSR_{Rayleigh,rain}(X,Ka,r) = \frac{\int_{v_{Rayleigh,rain}}^{v_{noise,X}} [S_X(v) - S_{Ka}(v)]dv}{v_{noise,X} - v_{Rayleigh,rain}} \quad (3.5)$$

where $v_{noise,X}$ is determined where the power spectral density is 10 dB above the X-band noise level. Thus the rain attenuation at Ka band from ground to *r* can be expressed as,

$$A_{rain}(Ka,r) = DSR_{Rayleigh,rain}(X,Ka,r) + A_{rain}(X,r) + A_{gas}(X,0,r) \quad (3.6)$$

where $A_{rain}(X,r)$ is the rain attenuation at X band from ground to *r*, $A_{gas}(X,0,r)$ is the gaseous attenuation at X band from ground to *r*. The millimeterwave propagation model (Liebe, 1985) is applied to estimate the gaseous attenuation at X, Ka and W bands in this study. Similarly, the rain attenuation at W band from ground to *r* can be written as,

$$A_{rain}(W,r) = DSR_{Rayleigh,rain}(Ka,W,r) + A_{rain}(Ka,r) + A_{gas}(Ka,0,r) \quad (3.7)$$

where $A_{rain}(\mathrm{Ka},\mathrm{r})$ is the rain attenuation at Ka band from ground to *r*, $A_{gas}(Ka,0,\mathrm{r})$ is the gaseous attenuation at Ka band from ground to *r*.

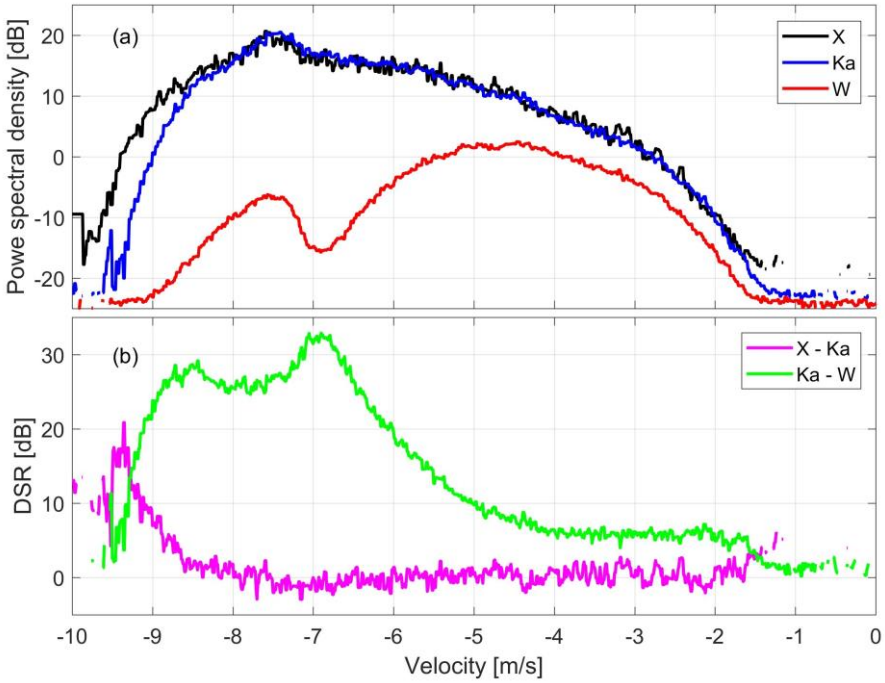

Figure 1: Doppler spectrums of X-, Ka- and W-band radars in rain (a), DSR for X/Ka and Ka/W in rain (b).

3.3 Melting layer location and attenuation

For single-polarized radar, the location of the melting layer is detected by using the reflectivity-based method. During, the multi-frequency radars are dual-polarized and capable of providing additional products such as ρ_{hv}, Z_{dr} and K_{dp}. In this study, we use the local dip of ρ_{hv} to detect the melting layer location.

Kneifel et al. (2016) presented the Rayleigh regime in DSR for Ka/W and X/Ka. As shown in Figue 2, the Doppler spectrum in snow is much narrower than that in rain. The flat Rayleigh regime is around -1.1 m/s ~ -0.8 m/s, which is narrower and noisier than that in rain. As expected, Ka band radar signal has longer wavelength, and the X/Ka DSR flat Rayleigh regime (-1.3 m/s ~ -0.8 m/s) is more significant than that for Ka/W. Thus, the X/Ka DSR in Rayleigh regime for snow at the range of *r* is defined as,

$$DSR_{Rayleigh,snow}(X,Ka,r) = \frac{\int_{v_{Rayleigh,snow,X/Ka}}^{v_{noise,X}} [S_X(v) - S_{Ka}(v)]dv}{v_{noise,X} - v_{Rayleigh,snow,X/Ka}} \quad (3.8)$$

where $v_{Rayleigh,snow,X/Ka}$ indicates the velocity which is 0.3 m/s (absolute value) smaller than the $v_{noise,X}$. For Ka/W DSR,

$$DSR_{Rayleigh,snow}(Ka,W,r) = \frac{\int_{v_{Rayleigh,snow,Ka/W}}^{v_{noise,W}} [S_{Ka}(v) - S_W(v)]dv}{v_{noise,W} - v_{Rayleigh,snow,Ka/W}} \quad (3.9)$$

where $v_{Rayleigh,snow,Ka/W}$ indicates the velocity which is 0.3 m/s (absolute value) smaller than the $v_{noise,W}$. For a meling layer locating from r_1 to r_2 ($r_1 < r_2$), the melting layer attenuation at Ka and W bands can be expressed as,

$$A_{ML}(Ka) = DSR_{Rayleigh,snow}(X,Ka,r_2) - A_{rain}(Ka,r_1) + A_{ML}(X) - A_{gas}(Ka,r_1,r_2) \quad (3.10)$$

$$A_{ML}(W) = DSR_{Rayleigh,snow}(Ka,W,r_2) - A_{rain}(W,r_1) + A_{ML}(Ka) + A_{gas}(Ka,r_1,r_2) - A_{gas}(W,r_1,r_2) \quad (3.11)$$

where $A_{ML}(X)$ indicates the melting layer attenuation at X band incorporating the attenuation from melting snow and the gaseous attenuation at X band throughout the melting layer. As stated before, gaseous attenuation at X band is very small, and is assumed to 0 dB. Matrosov et al. (2008) presented the two-way melting layer attenuation at X-, Ka-, and W-bands as

$$A_{ML}(X) = 0.048R^{1.05} \quad (3.12)$$

$$A_{ML}(Ka) = 0.66R^{1.1} \quad (3.13)$$

$$A_{ML}(W) = 2.6R^{0.87} \quad (3.14)$$

where R is the rain rate (mm/h). Thus,

$$\frac{A_{ML}(X)}{A_{ML}(Ka)} = \frac{1}{13.75R^{0.05}} \ll A_{ML}(Ka)\ (R > 0.1\ mm/h) \qquad (3.15)$$

(3.15) indicates that the melting layer attenuation at Ka band is much larger than that at X band for normal rainfall. Thus, the uncertainty from using the modelled relation for X-band is trivial in estimating Ka band attenuation.

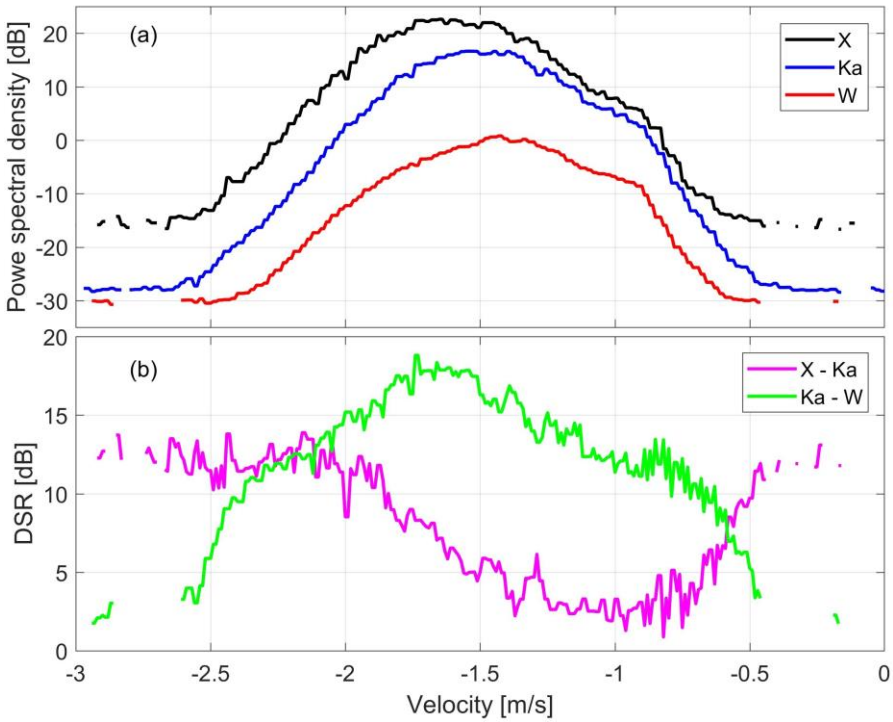

Figure 2: Doppler spectrums of X-, Ka- and W-band radars in snow (a), DSR for X/Ka and Ka/W in snow (b).

3.4 Rayleigh scatters in the cloud top

Except for searching the narrow Rayleigh regime in X/Ka and Ka/W DSR, ice crystals at cloud top can be good Rayleigh scatters at W band as well as at Ka band. Thus the DWR technique could also be utilized to estimate melting layer attenuation. (3.10) and (3.11) could be rewritten as,

$$A_{ML}(Ka) = Z_X(r_3) - Z_{Ka}(r_3) - [A(Ka, r_2, r_3) - A(X, r_2, r_3)] - A_{rain}(Ka, r_1) + A_{ML}(X) - A_{gas}(Ka, r_1, r_2) \qquad (3.16)$$

$$A_{ML}(W) = Z_{Ka}(r_3) - Z_W(r_3) - [A(Ka, r_2, r_3) - A(W, r_2, r_3)] - A_{rain}(W, r_1) + A_{ML}(Ka) + A_{gas}(Ka, r_1, r_2) - A_{gas}(W, r_1, r_2) \qquad (3.17)$$

where $Z_X(r_3)$, $Z_{Ka}(r_3)$, and $Z_W(r_3)$ are radar reflectivity at the range of r_3 (cloud top) for X, Ka and W band radars, respectively; $A(\mathrm{X}, r_2, r_3)$, $A(Ka, r_2, r_3)$ and $A(\mathrm{W}, r_2, r_3)$ are the integrated total attenuation from melting layer top r_2 to cloud top r_3, recpectively. The total attenuation above the melting layer contains the attenuation from dry snow, gaseous attenuation and possibly-existed supercooled water. For this event, only gaseous attenuation is considered.

4 Results

The stratiform rainfall in 12th June 2016 was observed by the multi-frequency radars. The melting layer attenuation is determined by utilizing (3.16) and (3.17). The retrieved melting layer attenuation is presented as a function of the X band radar reflectivity at the rain top (bottom of the melting layer). The rain rate in (3.13) is converted in to the radar reflectivity by using the Marshall-Palmer relation (Marshall and Palmer, 1948), which was used in (Matrosov, 2008). As shown in Figure 3, the measured melting layer attenuation is well matched with the model developed by Matrosov (2008). The increase of the Ka-band attenuation is also well characterized by the increasing radar reflectivity. Figure 4 presents the melting layer attenuation at W band. The measurements in general agree with the modelled ones well, especially for light precipitation (Z_X <17). For relatively intense precipitation, the model seems to underestimate the melting layer attenuation.

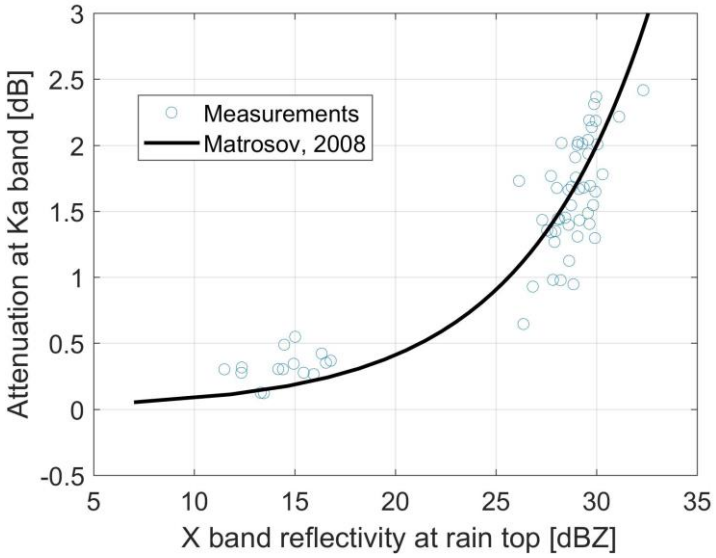

Figure 3: Ka-band melting layer attenuation

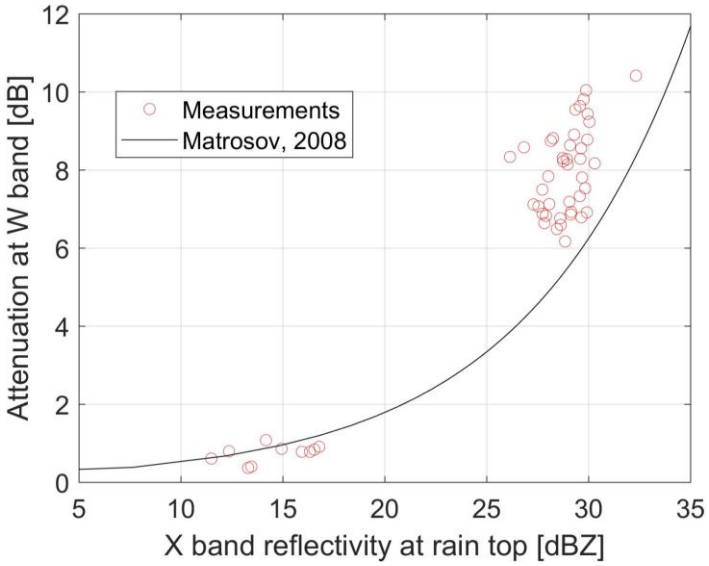

Figure 4: W-band melting layer attenuation

Acknowledgement

We would like to thank the personnel of Hyytiälä station and Matti Leskinen for their support in field observation. Dr. Stefan Kneifel is acknowledged for fruitful discussions. The research of HL and DM was supported by Academy of Finland (Grant no. 305175) and the Academy of Finland Finnish Center of Excellence program (Grant no. 307331). HL was also funded by China Scholarship Council. The instrumentation used in this study was supported by NASA Global Precipitation Measurement Mission ground validation program and by the Office of Science U.S. Department of Energy ARM program. The data used in this study are available from DOE ARM archives.

References

Bellon, A., I. Zawadzki, and F. Fabry, 1997: Measurements of melting layer attenuation at X-band frequencies, *Radio Sci.*, 32(3): 943–955.

Fabry F. and Szyrmer W., 1999: Modeling of the melting layer. Part II: Electromagnetic. *J. Atmos. Sci.*, 56(20): 3593-3600.

Fabry F. and Zawadzki I., 1995: Long-term radar observations of the melting layer of precipitation and their interpretation, *J. Atmos. Sci.*, 52(7): 838-851.

Hou A. Y., R. K. Kakar, S. Neeck, et al., 2014: The global precipitation measurement mission. *Bull. Am. Meteorol. Soc.*, 95(5): 701-722.

Illingworth A. J., H. W. Barker, A. Beljaars, et al., 2015: The EarthCARE satellite: The next step forward in global measurements of clouds, aerosols, precipitation, and radiation. *Bull. Am. Meteorol. Soc.*, 96(8): 1311-1332.

Illingworth A. J., R. J. Hogan, E. J O'connor., et al., 2007: Cloudnet: Continuous evaluation of cloud profiles in seven operational models using ground-based observations. *Bull. Am. Meteorol. Soc.*, 88(6): 883-898.

Johnson B. T., W. S. Olson, and G. Skofronick-Jackson, 2016: The microwave properties of simulated melting precipitation particles: sensitivity to initial melting. *Atmos. Meas. Tech.*, 2016, 9(1): 9.

Kneifel, S., P. Kollias, A. Battaglia, et al., 2016: First observations of triple-frequency radar Doppler spectra in snowfall: Interpretation and applications, *Geophys. Res. Lett.*, 43, 2225–2233, doi:10.1002/2015GL067618.

Kneifel, S., A. von Lerber, J. Tiira, et al., 2015: Observed relations between snowfall microphysics and triple-frequency radar measurements, *J. Geophys. Res. Atmos*., 120(12), 6034–6055, doi:10.1002/2015JD023156.

Kollias P. and Albrecht B., 2005: Why the melting layer radar reflectivity is not bright at 94 GHz, *Geophys. Res. Lett.*, 32, L24818, doi:10.1029/2005GL024074.

Leinonen J. and von Lerber A., 2018: Snowflake melting simulation using smoothed particle hydrodynamics. *J. Geophys. Res. Atmos*., 123(3): 1811-1825.

Liebe H. J., 1985: An updated model for millimeter wave propagation in moist air. *Radio Sci.*, 20(5): 1069-1089.

Marshall J. S. and Palmer W. M., 1948: The distribution of raindrops with size, *J. Meteorol.*, 5(4): 165–166.

Matrosov, S. Y.., 2008: Assessment of radar signal attenuation caused by the melting hydrometeor layer, *IEEE Trans. Geosci. Remote Sens.*, 46(4): 1039-1047.

Nakamura K, Y. Kaneko, K. Nakagawa, et al., 2018: Measurement Method for Specific Attenuation in the Melting Layer Using a Dual Ka-Band Radar System. *IEEE Trans. Geosci. Remote Sens.*, 56(6): 3511-3519.

Petäjä, T., et al., 2016: BAECC: A field campaign to elucidate the impact of biogenic aerosols on clouds and climate, *Bull. Amer. Meteor. Soc.*, 97(10), 1909–1928, doi:10.1175/BAMS-D-14-00199.1.

Sassen, K., J. R. Campbell, J. Zhu, P. Kollias, M. Shupe, and C. Williams, 2005: Lidar and triple-wavelength Doppler radar measurements of the melting layer: A revised model for dark- and brightband phenomena, *J. Appl. Meteorol.*, 44, 301 – 312.

Sekelsky S. M., W. L. Ecklund and K. S. Gage., 1999: Multi-frequency radar observations of the melting layer//Geoscience and Remote Sensing Symposium, IGARSS'99 Proceedings. IEEE 1999 International. IEEE, 1: 705-707.

Stephens G. L., Vane D. G., Boain R. J., et al., 2002: The CloudSat mission and the A-Train: A new dimension of space-based observations of clouds and precipitation. *Bull. Am. Meteorol. Soc.*, 83(12): 1771-1790.

Szyrmer W. and Zawadzki I., 1999: Modeling of the melting layer. Part I:Dynamics and microphysics, *J. Atmos. Sci.*, 56(20): 3573-3592.

Tridon, F., A. Battaglia, and P. Kollias, 2013: Disentangling mie and attenuation effects in rain using a Ka-W dual-wavelength Doppler spectral ratio technique, *Geophys. Res. Lett*., 40(20), 5548–5552, doi:10.1002/2013GL057454.

von Lerber A., D. Moisseev, J. Leinonen, et al., 2015: Modeling radar attenuation by a low melting layer with optimized model parameters at C-ban. *IEEE Trans. Geosci. Remote Sens.*, 53(2): 724-737.